Cost-Based Adaptive Droop Control Strategy for VSC-MTDC system

Sungyoon Song, *Student Member, IEEE*, Roy A. McCann, *Senior Member, IEEE*, and Gilsoo Jang, *Senior Member, IEEE*

***Abstract*—This study proposes a cost-based adaptive (CBA) droop control strategy for use in a voltage source converter (VSC)-based multi-terminal high voltage direct current (MTDC) system. Rather than using a fixed droop gain, we suggest the CBA droop control scheme, which reduces the total incremental generation cost of ac systems, while sharing the burden based on the available capacity of VSCs at the post-contingency-steady-state operating point. Following a certain VSC outage in the MTDC system, unbalanced power is allocated based on the equal incremental cost principle to reduce the total active power generation cost. The results were verified through a transient simulation on an MTDC system with four monopole VSCs, and outage contingency scenarios were presented with three groups of generation cost curves. The results indicate that the CBA droop control strategy can provide greater contributions to the economic operation of the MTDC system, while achieving robust control.**

***Index Terms*—Adaptive droop control, equal incremental cost principle, lagrangian method, VSC-MTDC.**

I. Introduction

FOR the integration of large amounts of renewable energy, voltage source converter (VSC)-based, high voltage direct current (HVDC) systems are currently the most appealing solution due to several advantages. In particular, there is a growing interest in the integration of renewable energy into multi-terminal direct current (MTDC) grids for better utilization, as opposed to connections by multiple point-to-point links, for better utilization. The transmission technology based on VSC-MTDC has many advantages as follows: realizes the independent control of active and reactive power [1]; provides black start capability and dynamic reactive power support [2]; improves power quality; reduces losses and footprint of the converter station; connects multiple ac systems or divide the ac system into multiple isolated power grids; and is suitable for grid-connected wind farms [3], weak grids, and urban grids. These advantages have led to its consideration as a key form of technology for the European Supergrid, which connects the ac grids of the North Sea countries [4], as well as for the two projects of Nanao wind farm integration [5], and Zhoushan islands interconnection in China [6].

For MTDC systems, the classical grid-side VSC control strategies can be classified into three types: master-slave control strategy [7], voltage margin control strategy [8], [9], and dc voltage droop control strategy [10]. The master-slave control strategy assigns only one VSC to control the dc voltage, while the others regulate the power injected into the ac grids. Specifically, it sets a main VSC as a power balance node to control the dc voltage, while the other converters control the active power. The disadvantage of this control scheme is the fact that the system will be paralyzed once the main VSC stops working [11], [12].

Considering the voltage margin control strategy, once the main VSC is out of service due to a fault or loss of communication, the other VSC begins to maintain the dc voltage. The secondary VSC can accomplish this by detecting the large deviation of the dc voltage and automatically switch from the constant active power mode to the dc voltage control mode.

Lastly, the voltage droop control strategy refers to the use of a dc grid with multiple VSCs operating in the dc voltage control mode. Thus, all the grid-side VSCs participate in dc voltage regulation based on the V-I characteristic, and the droop gains determine the power ratio. Thus, if one VSC is lost, the entire dc system can continue to function. In the voltage droop control strategy, fixed droop gains, primarily based on the individual ratings of the VSCs, have mainly been used [10]. VSCs will maintain constant power outputs until the droop gains are changed manually; therefore, this procedure reduces system operation flexibility. Accordingly, several authors have presented various adaptive droop control strategies to achieve their respective goals, as shown in Fig. 1.

For example, active power-dc voltage droop control, in which the reference of the voltage square is modified by active power droop, is proposed in [13]; dc current–dc voltage droop control is proposed in [14]. Furthermore, an adaptive droop control scheme for appropriate power sharing accounts for the available headroom (difference between the rated capacity and actual loading), and can avoid possible overloading [15], [16]. It can share the burden according to the available headroom of the converter station at post-contingency-steady-state operating points. Additionally, adaptive droop control strategies to minimize dc system loss [17] and to support frequency [18] are suggested,

Manuscript received October 22, 2019; revised March 3, 2020 and May 6, 2020; accepted June 9, 2020. Date of publication June 19, 2020; date of current version January 6, 2021. This work was supported in part by National Research Foundation undergrant 2017K1A4A3013579 and in part by the Human Resources Program in Energy Technology of the Korea Institute of Energy Technology Evaluation and Planning granted financial resource from the Ministry of Trade, Industry and Energy, Republic of Korea, under Grant 20174030201540. *(Corresponding author: Gilsoo Jang.)*

Sungyoon Song and Gilsoo Jang are with the School of Electrical Engineering, Korea University, Seoul (e-mail: blue6947@korea.ac.kr; gjang@korea.ac.kr).

Roy A. McCann is with the School of Electrical Engineering, Arkansas University, Fayetteville (e-mail: rmccann@uark.edu).

Color versions of one or more of the figures in this article are available online at http://ieeexplore.ieee.org.

Digital Object Identifier 10.1109/TPWRS.2020.3003589

0885-8950 © 2020 IEEE. Personal use is permitted, but republication/redistribution requires IEEE permission.
See https://www.ieee.org/publications/rights/index.html for more information.

Authorized licensed use limited to: University of Arkansas. Downloaded on March 01,2022 at 20:42:25 UTC from IEEE Xplore. Restrictions apply.

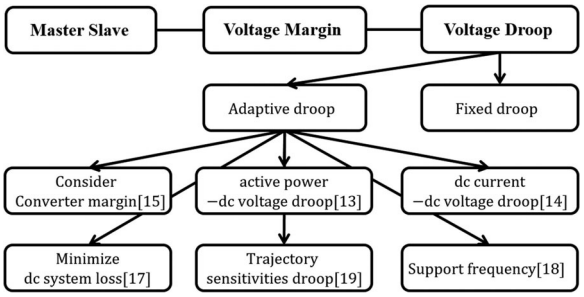

Fig. 1. Several voltage droop control strategies for MTDC system.

respectively. Recently, a trajectory-sensitivity-analysis based approach was also presented to impose the constraints on the adaptive droop gains [19], which was essential for the proposed droop scheme because certain settings of the droop gains may lead to instability of the ac system.

Furthermore, some researchers have focused on the economic power sharing in a VSC-based microgrid. A power system operator is obligated to apply a function of economic power sharing, because the current challenge in many power systems is the high cost of operation due to the high penetration of renewable energy. To develop an economical droop gain, various model-based cost minimization methods [20] have been introduced. However, they require network observation, relying heavily on remote monitoring. Accordingly, a real-time optimization method using energy management systems (EMS) [21] has been presented. However, the stability of the dc link and the available headroom of the converter stations have not been considered. To eliminate the need for remote monitoring, decentralized control strategies for multiple VSCs with no communication link have been addressed [22], [23]; however, accuracy can be compromised particularly when new resources are connected to the network. Thus, the optimal increment cost value cannot be derived because the controllers are only activated based on the variation of the frequency and voltage amplitude of the microgrid.

Considering these factors, this study proposes a cost-based adaptive (CBA) droop scheme, which can reduce the total generation cost of ac systems by EMS while achieving robust control. The problem is formulated by introducing the impact of dc voltage droop gain on the converter output power, and the economic power sharing methodology for MTDC is generalized in an inter-area power system. Converter outputs are implemented online through adjustments to droop characteristics within a constraint. The proposed CBA droop control strategy has several advantages:

1) It has the functionality of driving the incremental cost of generation to a consensus value.
2) In terms of the equal incremental cost principle, the total active power generation cost to regulate the dc grid voltage can be reduced when one VSC station is lost.
3) It eliminates the possibility of switching to a constant power control mode when operating in dc voltage droop control by locally adjusting the dc voltage droop gain.
4) It can select appropriate droop gains to satisfy various conditions associated with a combination of several types of generation while achieving robust control.
5) It can be further utilized to control inter-area power system operation.
6) It is a feasible interim option before the implementation of more complex schemes in an MTDC system.

In this study, this issue is perceived relative to dynamic control rather than power flow; hence, results from the dc grid shows stable voltage because constraints, as well as contingent scenarios are considered. This paper is organized as follows: the modeling procedure of VSC-MTDC is followed by the fixed and conventional adaptive droop control strategies introduced in Section II. In Section III, the proposed CBA droop control scheme and the online operation strategy are introduced. Finally, a simulation of the developed model with the proposed control scheme is presented in Section IV through PSCAD/EMTDC and Power System Simulator for Engineering (PSSE).

II. Conventional Droop Control Strategies of VSC-MTDC System

A. Converter Modeling

The general structure of the VSC-MTDC system with four terminals is shown in Fig. 2 (the dashed lines illustrate the proposed CBA droop scheme). The modeling procedure is similar to the approach used in [13], [24], [25], which is described here briefly. Each ac system is modeled as a voltage source connected to a VSC-MTDC, while for the dc system, each terminal is connected to a dc cable, which connects the rectifier and inverter sides together. The ac system connected to the MTDC grid is modeled in a synchronously rotating reference *d-q* frame, and the *q*-axis is locked with the ac voltage to ensure decoupled control of the active and reactive power. The dynamics of the ac side of the converter in the *d-q* frame can be expressed as follows:

$$\begin{bmatrix} v_1^d \\ v_1^q \end{bmatrix} - \begin{bmatrix} v_2^d \\ v_2^q \end{bmatrix} = R \begin{bmatrix} i_1^d \\ i_1^q \end{bmatrix} + L\frac{d}{dt}\begin{bmatrix} i_1^d \\ i_1^q \end{bmatrix} + \begin{bmatrix} -\omega L i_1^q \\ \omega L i_1^d \end{bmatrix}, \quad (1)$$

$$\begin{bmatrix} i_1^d \\ i_1^q \end{bmatrix} - \begin{bmatrix} i_2^d \\ i_2^q \end{bmatrix} = C\frac{d}{dt}\begin{bmatrix} v_2^d \\ v_2^q \end{bmatrix} + \begin{bmatrix} -\omega C v_2^q \\ \omega C v_2^d \end{bmatrix}. \quad (2)$$

where v_2 is the three-phase output voltage at the point common coupling (PCC) and v_1 is the voltage at the converter. Furthermore, R, C and L are the resistance, *LC* filter capacitance, and inductance, respectively; while i_1 and i_2 are the currents flowing through the ac system and the three-phase current flowing through the inductor, respectively. The symbol ω is the angular frequency of the ac voltage at the PCC. The reference voltage generated by the inner current control loop is transformed back into the abc frame and used for pulse width modulation (PWM) in order to produce the desired converter three-phase voltage.

When aligning the *d*- axis along with the PCC voltage, the instant active and reactive powers transferred from the converter to the ac grid are proportional to grid *d*- and *q*-axis currents as shwn by:

$$P_{VSC} = v_2^d i_2^d + v_2^q i_2^q = v_2^d i_2^d \quad = v_2^d i_1^d - v_2^d i_C^d. \quad (3)$$

$$Q_{VSC} = v_2^q i_2^d - v_2^d i_2^q = -v_2^d i_2^q \quad = -v_2^d i_1^q + v_2^d i_C^q. \quad (4)$$

Authorized licensed use limited to: University of Arkansas. Downloaded on March 01,2022 at 20:42:25 UTC from IEEE Xplore. Restrictions apply.

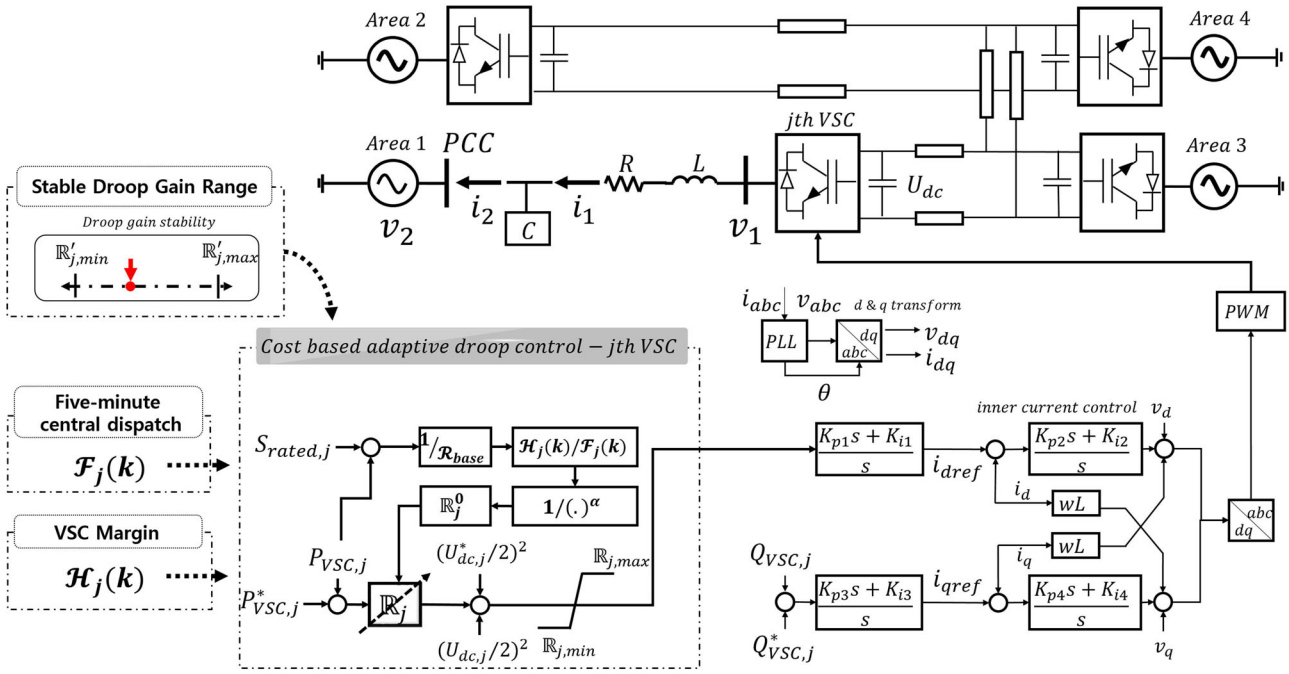

Fig. 2. The cost-based adaptive droop scheme for VSC-MTDC system.

where i_C^{dq} is the d- and q-axis capacitor current. Following the decoupled current control strategy, the active and reactive powers are controlled by the d- and q-axis currents. The simple equations presented above are some of the main reasons for using the d-q current control as the fastest inner control [25].

Note, capacitor currents are basically constant when the change in the grid voltage is insignificant, and the steady-state active and reactive powers at PCC can be obtained from the complex power equation as follows:

$$P_{VSC} + jQ_{VSC} = v_2^{dq}\left(i_2^{dq}\right)^*. \tag{5}$$

Considering $v_2^{dq} = v_2^d + j0$ because the d-axis is aligned along with the PCC voltage, and $v_1^{dq} = v_1^d + jv_1^q$, the current i_2^{dq} can be solved using (1) and (2) when neglecting the resistor as follows:

$$i_2^{dq} = \frac{v_1^q}{wL} + j\left(\frac{v_2^d - v_1^d}{wL} - v_2^d wC\right). \tag{6}$$

When applying (6) to the complex power equation, the active and reactive powers can be calculated as follows:

$$P_{VSC} = v_2^d v_1^q / wL. \tag{7}$$

$$Q_{VSC} = \left(v_2^d\right)^2 wC - v_2^d\left(v_2^d - v_1^d\right)/\,wL. \tag{8}$$

The equation represents the active power, and reactive powers can be controlled by the d- and q-axis voltage.

B. Fixed Droop Control Strategy of the MTDC System [10]

For an MTDC system with more than two grid-side VSCs, all of the remaining ones are desired to be responsible for the power imbalance after an outage of a certain VSC. Thus, all grid-side VSCs should operate in dc voltage control mode, as opposed to following their respective active power references in the droop control strategy. It is assumed that there are a total of N grid-side VSCs, where the jth VSC takes the dc voltage droop scheme; when unbalanced power occurs in the dc grids, the operation point moves from $P_{VSC,j} - U_{dc}$ to $P'_{VSC,j} - U'_{dc}$, and the unbalanced power ΔP_{up} is represented by the following:

$$\Delta P_{up} = P'_{VSC,N} - P_{VSC,N} = \sum_{j=1}^{N} \Delta P_{VSC,j}. \tag{9}$$

The dc voltage variation, ΔU_{dc}, occurs due to the input/output variables at another steady-state point in terms of the initial steady-state conditions:

$$\begin{aligned}\Delta U_{dc} &= U'_{dc} - U_{dc} = \mathbb{R}_N\left(P'_{VSC,N} - P_{VSC,N}\right)\\ &= \mathbb{R}_N \Delta P_{VSC,N}.\end{aligned} \tag{10}$$

The symbol $\mathbb{R}$ refers to the fixed droop gain and has a unit of kV/MW, it can be calculated by the following [10]:

$$\mathbb{R}_N = \sum_{j=1}^{N} \mathbb{R}_j = \sum_{j=1}^{N} \frac{U_{dc}}{S_{rated,j}}. \tag{11}$$

where $S_{rated,j}$ is the rated power at the jth VSC, and U_{dc} is the rated dc voltage of the dc terminal, respectively. In a

Authorized licensed use limited to: University of Arkansas. Downloaded on March 01,2022 at 20:42:25 UTC from IEEE Xplore. Restrictions apply.

dc grid without any loss, all dc bus voltages would be equal; thus, when the VSC stations have the same size of $\mathbb{R}$, then the unbalanced power will be shared equal to the grid-side converter station. From (9) and (10), the unbalanced active power with the respective dc voltage droop slope is allocated at the *j*th VSC as follows:

$$\Delta P_{up} = \Delta U_{dc} \sum_{j=1}^{N} \frac{1}{\mathbb{R}_j} = \mathbb{R}_N \Delta P_{VSC,N} \sum_{j=1}^{N} \frac{1}{\mathbb{R}_j}, \tag{12}$$

By rearranging (12), the shared active power with slope $\mathbb{R}_N$ is expressed as follows:

$$\Delta P_{VSC,N} = \frac{\Delta P_{up}}{\mathbb{R}_N \sum_{j=1}^{N} \frac{1}{\mathbb{R}_j}}. \tag{13}$$

From (13), considering VSCs with the same capacity, the unbalanced power will be allocated equally. Here, the *j*th VSC with a larger $\mathbb{R}_j$ indicates that smaller unbalanced power will be shared, while a smaller $\mathbb{R}_j$ indicates that larger unbalanced power will be shared. However, the fixed droop control does not consider the headroom of all VSCs in actual operating conditions, which leads to a certain VSC switching to the constant power control mode, making the other VSC lose its corresponding ability [16].

C. Adaptive Droop Control Strategy of the MTDC System

As mentioned in section B, the fixed droop strategy has some disadvantages; an adaptive droop control strategy has been proposed using $\mathbb{R}_j \rightarrow \mathbb{R}'_j$. This strategy is advantageous because autonomous power sharing is efficiently executed at both, steady-state operating points and post-contingency, and the dc link is well maintained with very little overshoot. Based on previous studies [10], [15], [19], the CBA droop strategy for economical MTDC system operation is introduced hereafter.

III. Cost-based Adaptive Droop Control Strategy

This section introduces the modified economic dispatch algorithm to determine a cost-based droop gain in a MTDC system. It has the ability to reduce the total active power generation cost following a certain VSC outage. The equal incremental cost principle is a suitable solution for use because the MTDC system is connected with multiple ac systems, which may have different generation cost functions. Thus, both the Lagrangian method and the equal incremental cost principle were applied in the CBA control strategy.

A. Equal Incremental Cost Principle

In general, it was assumed that there are *M* generators in the ac system that supply power to the designated *j*th VSC, and the *l*th generator has a respective cost function. In order to minimize the total active power generation cost while satisfying the power balance and generation constraint, the object function is expressed as follows [26]–[28]:

$$Min \sum_{l=1}^{M} C_l\left(P_l\right) = \sum_{l=1}^{M} \left(a_l P_l^2 + b_l P_l + c_l\right), \tag{14}$$

$$\sum_{l=1}^{M} P_l = P_D, \quad P_l^{min} \le P_l \le P_l^{max}. \tag{15}$$

where P_l is the active power of the *l*th generators, $C_l(P_l)$ is the cost function of *l*th generators, and a_l, b_l and c_l are the incremental cost gains of the generators. P_D is the total active load demand in the ac system. P_l^{min} and P_l^{max} are the lower and upper limits of active power generation of the *l*th generators, respectively. In order to solve the economic dispatch issue, the Lagrangian method is applied; the terms can be expressed as follows:

$$L\left(P_1, \ldots P_M\right) = \sum_{l=1}^{M} C_l(P_l) + \lambda \left(P_D - \sum_{l=1}^{M} P_l\right), \tag{16}$$

where λ is the well-known Lagrange multiplier, and the first-order optimal condition is provided as follows:

$$\frac{\partial L}{\partial P_l} = \frac{\partial C_l\left(P_l\right)}{\partial P_l} - \lambda = 2a_l P_l + b_l - \lambda = 0, \tag{17}$$

$$\frac{\partial L}{\partial \lambda} = P_D - \sum_{l=1}^{M} P_l = 0, \tag{18}$$

According to (17), the variable λ is indeed an optimal incremental cost and satisfies the following:

$$\lambda = 2a_l P_l + b_l, \tag{19}$$

$$P_l = \frac{\lambda - b_l}{2a_l}, \tag{20}$$

where λ is the optimal incremental cost of the *l*th generator. After substituting (20) into (18), the optimal incremental cost of units can be calculated as follows:

$$\lambda = \left(\sum_{l=1}^{M} \frac{1}{2a_l}\right)^{-1} \sum_{l=1}^{M} P_l + \left(\sum_{l=1}^{M} \frac{1}{2a_l}\right)^{-1} \sum_{l=1}^{M} \frac{b_l}{2a_l}. \tag{21}$$

The generators that operate within the power generation limits each have an incremental cost of $\frac{\partial C_l(P_l)}{\partial P_l}$, whereas generators operating on their upper or lower generation limits have an incremental cost of $\frac{\partial C_l(P_l)}{\partial P_l}\|_{P_l=P_l^{max}}$ or $\frac{\partial C_l(P_l)}{\partial P_l}\|_{P_l=P_l^{min}}$, respectively. Note, that the wind reserve can also be considered in this economic dispatch calculation. A wind farm with a larger power reserve uncertainty is assigned a larger penalty coefficient. This penalty coefficient intentionally scales up the cost of its power reserve in the cost function; therefore, the competitiveness of wind farms changes when a penalty factor is assigned to the wind farm that has the highest probability of power reserve unavailability for next dispatch cycle.

B. Introduction of the CBA Droop Control Strategy

Based on the equal increment cost principle, this section proposes a feedback loop from the conventional economic dispatch algorithms to the MTDC system for determining a cost-based droop gain. The optimal incremental cost for the *j*th area may change in 1- or 5-minute dispatch cycle based on unit commitment and economic dispatch decision making; thus, a 1- or 5-minute central dispatch result should be shared with the

Authorized licensed use limited to: University of Arkansas. Downloaded on March 01,2022 at 20:42:25 UTC from IEEE Xplore. Restrictions apply.

communication system of MTDC. Furthermore, the VSC margin must be simultaneously considered to create a CBA droop gain; therefore, two pieces of information are updated as follows:

$$Online_{j\in N} = \{Online_1(k), \ldots, Online_N(k)\}, \quad (22)$$

$$\mathcal{H}_{j\in N} = \{\mathcal{H}_1(k), \ldots, \mathcal{H}_N(k)\}. \quad (23)$$

where $Online_j$ is an online economic dispatch result for the *j*th area, which is connected to the *j*th VSC at the *k*th time. $\mathcal{H}_j$ is the available headroom of the *j*th VSC at the *k*th time. It was assumed that each ac system has *M* generators; (21) can be modified by the economic dispatch result $Online(k)$ as follows:

$$\lambda_j^*(k) = \left(\sum_{l=1}^{j,M} \frac{1}{2a_{j,l}}\right)^{-1} \left(\sum_{l=1}^{j,M} P_{j,l} + \Delta P_v\right) + \left(\sum_{l=1}^{j,M} \frac{1}{2a_{j,l}}\right)^{-1} \sum_{l=1}^{j,M} \frac{b_{j,l}}{2a_{j,l}}. \quad (24)$$

where $\lambda_j^*(k)$ is the optimal incremental cost of generators for the load and dc grid voltage regulation at the *j*th VSC at the *k*th time, and ΔP_v is the total active power loss in the dc grid after a certain VSC outage. It is assumed that the cost curve of unit *l* is quadratic and there are four VSCs in the MTDC system, and four constant values of λ^* will be derived. Then, λ_j^* is normalized to assign a droop gain to the *j*th VSC proportional to the total generation cost of the ac system. The final cost factor $\mathcal{F}_j$ at the *j*th VSC is defined as follows:

$$\mathcal{F}_j(k) = \frac{\lambda_j^*(k)}{\sum_j^N \lambda_j^*(k)}, \quad (25)$$

Note, while the total cost of *N* ac systems can be reduced, it does not reach the minimum. The optimization model including *N* ac systems can minimize the total cost, but this type of multi-agent optimization requires an extended amount of time to solve the problem. The droop gain $\mathbb{R}$ should be changed immediately after a fault such that the normalization of λ_j^* value, which is updated by EMS in a 1- or 5-minute dispatch cycle, is utilized by (25). Once both $\mathcal{F}_j(k)$ and $\mathcal{H}_j(k)$ are updated via the dispatch algorithms and the communication system, the CBA droop gain can be created. By combining the existing adaptive droop formula [15] and (25), the proposed droop gain $\mathbb{R}_j'$ can be expressed as follows:

$$\mathbb{R}_j'(k) = \mathbb{R}_j^0 \times \left(\frac{\mathcal{R}_{base}}{\mathcal{H}_j(k)} \times \mathcal{F}_j(k)\right)^{\alpha}. \quad (26)$$

where $\mathcal{H}_j$ is the available headroom of the *j*th VSC, $\mathcal{R}_{base}$ is the maximum value of all VSC ratings, and $\mathbb{R}_j^0$ is a nominal droop gain. Therefore, the unit $\mathbb{R}_j'$ is p.u. α is a user-defined positive constant, and it is used to adjust the $\mathbb{R}_j'$ value to a stable operation point. If $\mathbb{R}_j'$ is not located in the stable droop gain range, α should be modified to ensure the performance and small-signal stability of the converter. In particular, dynamics of the control system in a grid-connected VSC become more complicated when connected to a weak grid, which is often associated with stability issues. Thus, a stability-constrained adaptive droop approach is required with a weak grid.

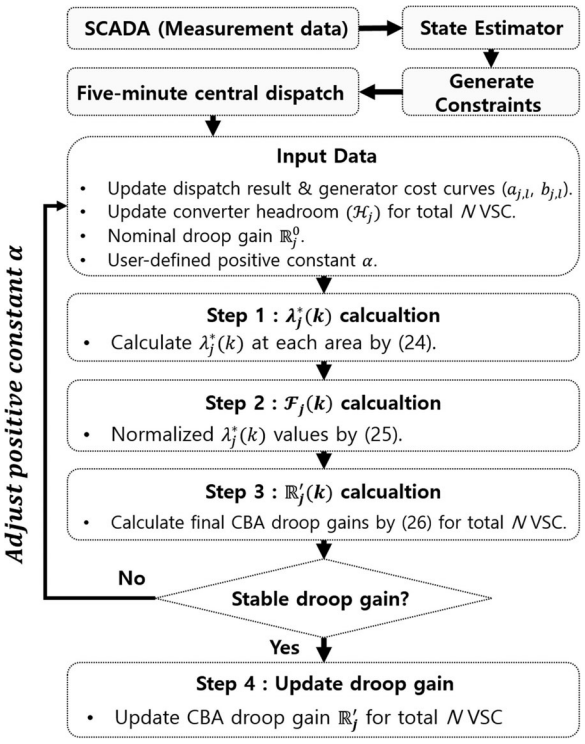

Fig. 3. Four steps for CBA droop gain update.

Considering (26), the VSCs that participate in the CBA droop control strategy have different $\mathcal{F}_j$ values at each economic dispatch cycle, and the cost factor $\mathcal{F}_j$ is the determinant of the droop gain $\mathbb{R}_j'$. $\mathbb{R}_j'$ becomes larger when the cost factor $\mathcal{F}_j$ is large; consequently, smaller unbalanced power is allocated to reduce the total generation cost. In contrast, when $\mathcal{F}_j$ is small, $\mathbb{R}_j'$ becomes smaller; consequently, large unbalanced power is shared in order to utilize inexpensive power after a VSC outage. Coincidentally, if the cost factor $\mathcal{F}_j$ is large while the headroom $\mathcal{H}_j$ is small, the updated $\mathbb{R}_j'$ would be the largest, and the smallest unbalanced power would be assigned to the VSC. Although the method requires an initial investment cost for communication systems, it can save on annual operating costs. The control block diagram and detailed procedure for updating the CBA droop gain are shown in Fig. 2 and Fig. 3, respectively.

The sequence of events followed in the proposed approach are listed as follows:

1) Use the nominal droop gains $\mathbb{R}_j^0$ at *k*th time as calculated based on the converter rating and stability.
2) Continue calculating both, the converter headroom $\mathcal{H}_j$ and the cost factor $\mathcal{F}_j$, based on the economic dispatch cycle. Note, $\mathcal{F}_j$ is dependent on the online dispatch results, the economic dispatch decision should be shared with the MTDC system.
3) Upon detection of a VSC outage, command the sample and hold function to invoke the updated $\mathbb{R}_j'$.

C. Droop Gain Stability Analysis of a Single VSC

The droop gain has a specific range for achieving acceptable operating points based on the damping ratios of the eigenvalues.

Authorized licensed use limited to: University of Arkansas. Downloaded on March 01,2022 at 20:42:25 UTC from IEEE Xplore. Restrictions apply.

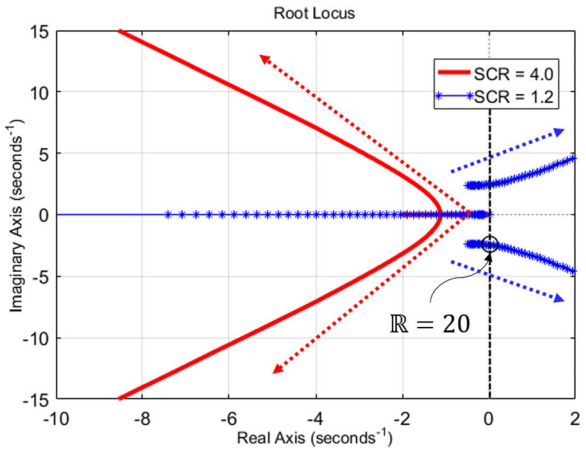

Fig. 4. Path of dominant eigenvalues as droop gain increase.

A complete survey of the droop stability analysis is beyond the scope of this study; we have provided a short summary here.

Several researchers have noted that a VSC with large gains that is connected to a weak ac grid is prone to instabilities when subjected to a disturbance [29]. This is because the high gain can easily generate an unstable eigenvalue with high proportional gains. Based on (1) and (2), the reduced third-order small-signal model of a single VSC can be written as follows:

$$\frac{d}{dt}\begin{bmatrix}\Delta x_1\\ \Delta x_2\\ \Delta\delta\end{bmatrix} = \mathbf{A}\begin{bmatrix}\Delta x_1\\ \Delta x_2\\ \Delta\delta\end{bmatrix}. \tag{27}$$

$$\frac{d\Delta x_1}{dt} = \Delta e_p, \frac{d\Delta x_2}{dt} = \Delta e_v, \frac{d\Delta\delta}{dt} = k_{PLL}\Delta v_2^q. \tag{28}$$

where Δe_p and Δe_v are the errors of the active power controller and voltage controller, respectively; and k_{PLL} is the PLL gain. The coefficient parameters of the matrix $\mathbf{A}$ can be found in [30], and see [30] for a detailed modeling procedure. As explained in [31], because the unstable modes resulting from the interaction between the VSC and the weak ac network is only on the order of several Hertz, the higher frequency dynamic behavior of the ac system network can be ignored. Furthermore, with this low frequency, the conductance of any filter capacitor at the PCC is negligible. Using the Cayley-Hamilton theorem, matrix $\mathbf{A}$ can be reduced further, the real part of the eigenvalues of the reduced model is shown in Fig. 4.

The unstable mode was significantly affected by the droop gains, particularly under SCR $= 1.2$. The system was unstable within certain droop gain ranges ($\mathbb{R} > 20$), and a larger gain would make the system unstable. Thus, the stable droop gain range in the CBA droop strategy must be predefined depending upon the system strength; the stability constraints of the droop gain of a converter under a certain VSC outage should be performed in an offline study [19].

IV. Simulation and Analysis

To clearly show the simplicity and efficiency of the proposed CBA droop strategy, this section considers the four-terminal dc system. First, the two kinds of structures and parameters of the VSC-MTDC for simulation are introduced. Next, the method in which the CBA droop control strategy is applied in the MTDC system from the analytical derivation is discussed.

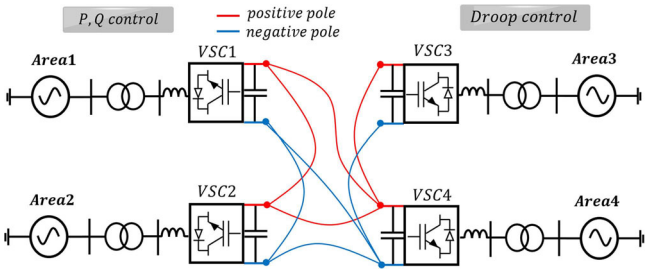

Fig. 5. Schematic diagram of VSC-MTDC.

TABLE I
Parameters of the VSC-MTDC System

	Item	Value
VSC3	Rated power (MVA)	600
	Nominal ac voltage (kV)	220
	Inductance (H)	5000
	Short circuit impedance (ohm,H)	0.1,0.015
	Transformer reactance (pu)	0.18
VSC4	Rated power (MVA)	600
	Nominal ac voltage (kV)	220
	Inductance (H)	5000
	Short circuit impedance (ohm,H)	0.8,0.017
	Transformer reactance (pu)	0.18
PI controller	Outer controller, k_{p1}	0.48
	Outer controller, k_{i1}	0.0067
	Current controller, k_{p2}	0.48
	Current controller, k_{i2}	0.0067
Dc voltage	Dc voltage (kV)	400
Dc cable	Length of line (km)	200
	Resistivity (ohm*m)	2.2e-8

TABLE II
Generator Cost Curves for the Two Scenarios

Area	Gen	Scenario 1	Scenario 2
3	1	$0.002P_1^2 + 0.2P_1 + 13$	$0.003P_1^2 + 0.2P_1 + 25$
	2	$0.003P_2^2 + 0.05P_2 + 5$	$0.003P_2^2 + 0.25P_2 + 2$
	3	$0.001P_3^2 + 0.1P_3 + 18$	$0.001P_3^2 + 0.1P_3 + 30$
	4	$0.004P_4^2 + 0.1P_4 + 24$	$0.003P_4^2 + 0.2P_4 + 14$
4	1	$0.002P_1^2 + 0.5P_1 + 25$	$0.004P_1^2 + 0.3P_1 + 5$
	2	$0.003P_2^2 + 0.1P_2 + 12$	$0.004P_2^2 + 0.2P_2 + 7$
	3	$0.005P_3^2 + 0.5P_3 + 30$	$0.004P_3^2 + 0.3P_3 + 13$
	4	$0.004P_4^2 + 0.4P_4 + 12$	$0.003P_4^2 + 0.2P_4 + 12$

A. Fixed Versus CBA Droop Control Scheme

1) System Structure: The study network established in PSCAD/EMTDC, consists of four monopole VSCs connected with 200 km dc cables, as shown in Fig. 5. The specifications of the converter and the controller parameters are listed in Table I. The cable parameters were obtained from a PSCAD generic model, and the surrounding ac systems were modeled using ideal 380 kV voltage sources; the equivalent resistances and inductances are 0.1 ohm and 0.015 H for area 3, respectively; 0.8 ohm and 0.017 H for area 4, respectively.

Authorized licensed use limited to: University of Arkansas. Downloaded on March 01,2022 at 20:42:25 UTC from IEEE Xplore. Restrictions apply.

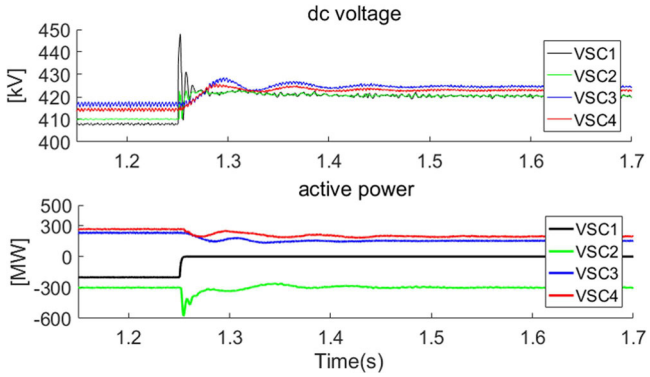

Fig. 6. DC link and active power for a fixed droop scheme following the outage of VSC1 in scenario 1.

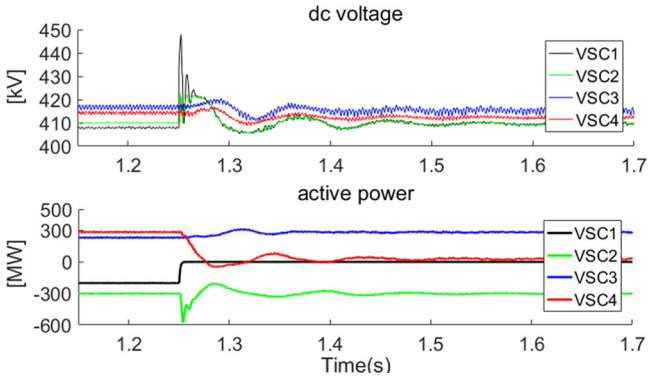

Fig. 7. DC link and active power for the CBA droop scheme following the outage of VSC1 in scenario 1.

TABLE III
COST FACTORS AND CBA DROOP GAINS IN SCENARIO 1

VSC	$\mathcal{F}_j$	$\mathbb{R}'_j$
3	0.3093	4.81
4	0.6907	11.14

In the initial state, VSC1 and VSC2 are considered to act as rectifiers that maintain the $P-Q$ control mode at the PCC. Conversely, stations VSC3 and VSC4 serve as grid-side inverters with a fixed droop scheme or the proposed CBA droop scheme and operate in $U_{dc}-Q$ control. Both VSC1 and VSC2 adopt $P-Q$ control to fairly compare the total generation cost between area 3 and 4. If necessary, any other VSC adopting droop control in MTDC system can be considered. The dc voltage was maintained at $\pm$400kV and the unequal loading conditions at the four VSCs were considered; and VSC1 outage (approximately 200 MW) was simulated for the two different scenarios. VSC1 and VSC2 rectifiers export approximately 200 MW and 300 MW, respectively, from the dc grid; while those of VSC3 and VSC4 import 230 MW and 280 MW, respectively, to the ac systems.

And, for the generator cost curves of two kinds of scenarios, it was assumed that the cost of the *l*th generator was approximated with a quadratic function, which takes the forms of (17), as shown in Table II. The total number of generators is set by $M=4$ at both areas, and four different types of generators have respective cost functions. The cost functions in Table II are all thermal power plant cost curves, which have units of USD/h.

2) Scenario 1: Regarding the fixed droop control strategy, the droop gains are determined by $\mathbb{R}_3, \mathbb{R}_4 = 5$ for converter performance, while considering the converter power ratings of VSC3 and VSC4. Considering VSC1 outage, the active power from the rectifier becomes 0 MW at $t=1.25\ s$, as shown by the black trace in Fig. 6. Therefore, the two inverters VSC3 and VSC4 lower their power in order to compensate for the loss of the rectifier (VSC1), as shown by blue and red lines in Fig. 6. In the fixed droop scheme, the burden is shared equally by the remaining two kinds of inverters; thus, VSC3 decreases its power from 230 MW to 150 MW, while VSC4 reduces its power from 280 MW to 200 MW, as shown by blue and red traces in Fig. 6. Results indicate that the active power fluctuation does not exceed the upper or lower limit with the fixed droop control. Because we focus on the impact of varying the cost factor $\mathcal{F}_j$ on the active power output, it is assumed that the headroom at each VSC is sufficiently acquired.

Furthermore, the dc link voltage of each converter station was observed, as shown in Fig. 6. The dc voltage increases following the rectifier outage, and the variation of the dc voltage error between the reference and measuring value at each VSC station is estimated to be approximately 2.5%.

In the proposed CBA droop strategy, the normalized cost factor $\mathcal{F}_j$ was first calculated based on the four different types of generator cost curves, as shown on the left side of Table II. For example, it is assumed that the total load of area 4 is 400 MW and given that $\sum_{l=1}^{4} P_l + \Delta P_v = 400\ \text{MW} - 200\ \text{MW} = 200\ \text{MW}$ in area 4, λ_4^* can be calculated by (24) as follows:

$$\begin{aligned}\lambda_4^* &= (1/0.004 + 1/0.006 + 1/0.01 + 1/0.008)^{-1} \times 200 \\ &\quad + (1/0.004 + 1/0.006 + 1/0.01 + 1/0.008) \\ &\quad \times (0.5/0.004 + 0.1/0.006 + 0.5/0.01 + 0.4/0.008) \\ &= 0.688.\end{aligned}$$

Based on the λ_3^* and λ_4^* values, the CBA droop gains $\mathbb{R}'_3$ and $\mathbb{R}'_4$ can be created by (26), respectively, as shown in Table III. Considering the stable range of $\mathbb{R}'_j$, the user-defined positive constant α was set to 0.85. Accordingly, the CBA droop gains were updated to be $\mathbb{R}'_3$ =4.81 for VSC3, and $\mathbb{R}'_4$ =11.14 for VSC4 in the economic dispatch cycle, as shown on Table III.

As shown by the red trace in Fig. 7, VSC4, which has a higher cost factor $\mathcal{F}_j$ value than VSC3, decreases its power to the MTDC grids by a greater value, since the incremental cost in the power market of area 4 is high. Thus, VSC3 increases its power to the MTDC grids from 230 MW to 280 MW, while VSC4 reduces its power from 280 MW to 30 MW as shown in Figs. 7 and 8.

By using a cost-based droop gain, the relatively inexpensive active power is flowing into the dc grid in order to regulate the dc link voltage, while relatively expensive power can be largely reduced. Furthermore, the CBA droop scheme can apparently reduce the total cost of area 4 by approximately 147.49 USD/h

Authorized licensed use limited to: University of Arkansas. Downloaded on March 01,2022 at 20:42:25 UTC from IEEE Xplore. Restrictions apply.

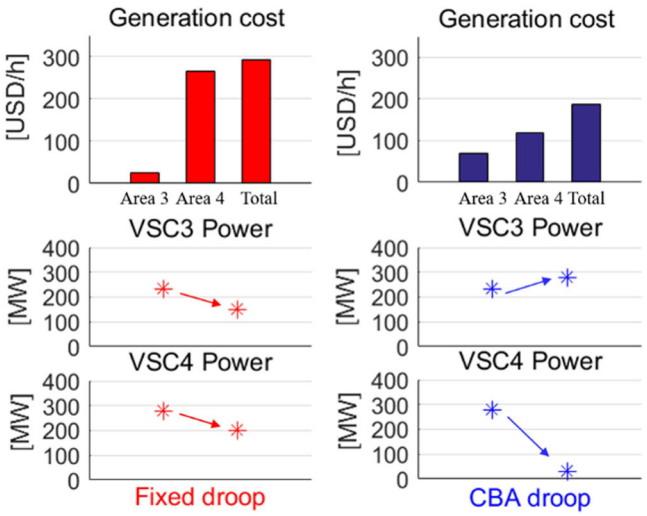

Fig. 8. Generation cost results and VSCs power change after contingency.

more than the fixed droop scheme, as shown by the red and blue bars in Fig. 8. For instance, the total incremental cost for area 4 adopting the fixed droop scheme can be calculated by (20) as follows:

$$P_1 = 125 \text{ MW}, P_2 = 150 \text{ MW}, \ P_3 = 50 \text{ MW}, \ P_4 = 75 \text{ MW}.$$

Total cost $= \sum_{l=1}^{4} C_l(P_l) = 93.75 + 82.5 + 37.5 + 52.5 = 266.25$ USD/h.

Conversely, the total cost for area 4 adopting the proposed CBA droop scheme can be calculated as follows:

$$P_1 = 58.7 \text{ MW}, P_2 = 105 \text{ MW}, \ P_3 = 23.5 \text{ MW},$$
$$P_4 = 41.8 \text{ MW}.$$

Total cost $= \sum_{l=1}^{4} C_l(P_l) = 36.29 + 44.19 + 14.5 + 23.77 = 118.7695$ USD/h.

Therefore, the total generation cost for the two ac systems can be reduced more than using the fixed droop control strategy, and it should be noted that the post-contingency-steady-state operating point results are consistent with the analytical values.

By adopting the CBA droop gain, the respective dc voltage of the VSCs was well maintained, within 0.01% error, as shown in Fig. 7; the respective reference dc voltage is controlled as well due to a much higher droop gain in VSC4 determined immediately after a rectifier outage. The final dc voltage values between the fixed and CBA droop are not the same because the total output active power sum for the two inverters is different at the post-contingency-steady-state. The proposed droop scheme does not deteriorate the dc link dynamics further than the fixed droop strategy, and economic power sharing is well reflected in this scheme. Furthermore, by observing the VSC power change results after a contingency, no converter violated their power rating because the capacity factor $\mathcal{H}_j$ was also included in (26), so power changes of VSC3 and VSC4 were deemed to be sufficiently acceptable for the converter limit.

TABLE IV
COST FACTORS AND CBA DROOP GAINS IN SCENARIO 2

VSC	$\mathcal{F}_j$	$\mathbb{R}'_j$
3	0.368	5.07
4	0.631	8.94

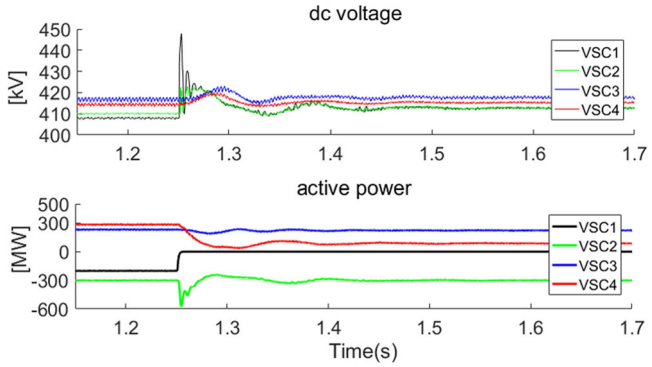

Fig. 9. DC link and active power for the CBA droop scheme following the outage of VSC1 in scenario 2.

3) Scenario 2: In the second scenario, both VSC1 and VSC2 maintain $P - Q$ control mode to be the same as in the first case, and the VSC1 rectifier outage is considered. The modified CBA droop gains of $\mathbb{R}'_3$ for VSC3, and $\mathbb{R}'_4$ for VSC4 are applied, based on the different generator cost curves, as shown on the right side of Table II. The normalized cost factors $\mathcal{F}_j$ were recalculated from the different unit scheduling results. It is assumed that the total load of area 4 is 400 MW and given that $\sum_{l=1}^{4} P_l + \Delta P_v = 400 \text{ MW} - 200 \text{ MW} = 200 \text{ MW}$, λ_4^* can be recalculated as follows:

$$\begin{aligned}\lambda_4^* &= (1/0.008 + 1/0.008 + 1/0.008 + 1/0.006)^{-1} \times 200 \\ &\quad + (1/0.008 + 1/0.008 + 1/0.008 + 1/0.006) \\ &\quad \times (0.3/0.008 + 0.2/0.008 + 0.3/0.008 + 0.2/0.006) \\ &= 0.615.\end{aligned}$$

Using λ_3^* and λ_4^* values, $\mathbb{R}'_3$ and $\mathbb{R}'_4$ were equal to $\mathbb{R}'_3 = 5.07$ for VSC3 and $\mathbb{R}'_4 = 8.94$ for VSC4, as shown in Table IV. Note, α is calculated by the droop grain stability of VSC. It can be seen from Table III and Table IV, the interval between $\mathbb{R}'_3$ and $\mathbb{R}'_4$ was narrower than that in the scenario 1.

As shown by the blue and red lines in Fig. 9, the active power from the rectifier apparently becomes 0 MW at $t = 1.25s$, and the two inverters reduce their power to regulate the dc link voltage. By using the $\mathcal{F}_3$ and $\mathcal{F}_4$ values, VSC4 reduces its power from 280 MW to 85 MW, and VSC3 maintains its active power at approximately 220 MW, as shown in Figs. 9 and 10.

Considering the impact of varying $\mathcal{F}_j$ on active power, the amount of reduced power differs from the scenario 1. VSC4, which has a smaller $\mathcal{F}_4$ than the scenario 1 (11.14 to 8.94), increases its active power from 30 MW to 85 MW. Thus, the total cost for area 4 adopting CBA droop gain differs from the

Authorized licensed use limited to: University of Arkansas. Downloaded on March 01,2022 at 20:42:25 UTC from IEEE Xplore. Restrictions apply.

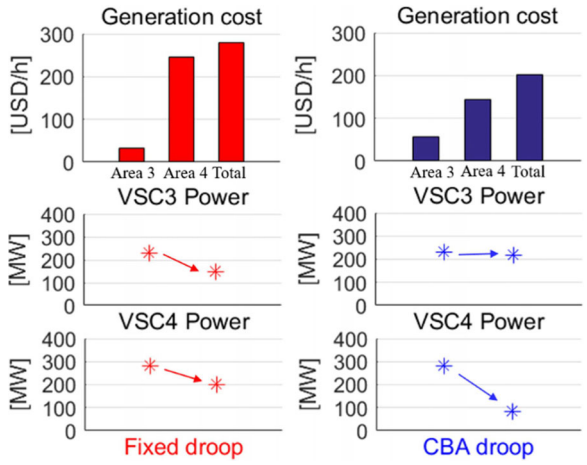

Fig. 10. Generation cost results and VSCs power change after contingency.

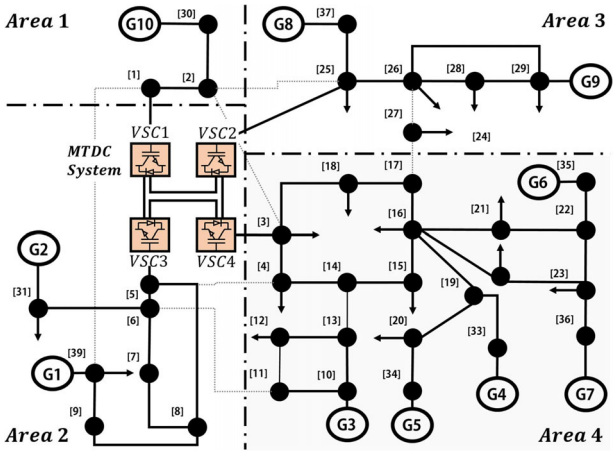

Fig. 11. Modified IEEE 39-bus standard test system.

first scenario as follows:

$$P_1 = 59 \text{ MW}, P_2 = 71 \text{ MW}, \ P_3 = 59.03 \text{ MW},$$
$$P_4 = 95.38 \text{ MW}.$$

Total cost $= \sum_{l=1}^{4} C_l(P_l) = 31.65 + 34.77 + 31.65 + 46.37 = 144.45$ USD/h.

Note, as $\mathcal{F}_i$ is reduced, a larger active power amount flows into the MTDC grids to reduce the total generation cost. Conversely, if $\mathcal{F}_i$ is increased, a smaller active power amount flows into the MTDC grids to avoid using relatively expensive active power. Compared to the fixed droop strategy, the CBA droop strategy reduces the incremental cost from 278.64 USD/h to 201.65 USD/h based on the second-generation list, as shown by the red and blue bars in Fig. 10. Apparently, a reduced total power generation cost can be achieved and meaningful power sharing at the post-contingency-steady-state operating point is possible. Note, the operating point for each VSC should be adjusted after a contingency to ensure proper power flow between regions.

B. Adaptive Droop Versus CBA Droop Scheme

1) System Structure: To escalate the effectiveness of the proposed strategy, the proposed CBA droop strategy is performed in IEEE-39 bus standard system in PSSE. The modified IEEE-39 bus standard system has 39 buses and 28 branches as it is, and the load bus follows an original value, as shown in [Fig. 11]. However, the MTDC system was newly attached at the 1, 3, 5 and 25 buses and the several ac transmission lines are switched off for grid separation. The specifications of the converter are listed in Table V.

Four VSCs maintain the droop control mode at the PCC, and VSC4 outage was simulated. VSC2 and VSC3 rectifiers export approximately 50 MW and 28 MW, respectively, from the dc grid; while those of VSC1 and VSC4 import 35 MW and 44 MW, respectively, to the ac systems.

As same as the section A, it was assumed that the cost of the *l*th generator was approximated with a quadratic function, as shown in Table VI. The total number of generators is set by $M = 1$ at area 1, and $M = 2$ at area 2 and 3, as shown in the Fig. 11. The cost functions in Table VI are all conventional power plant cost curves, which have units of USD/h.

TABLE V
PARAMETERS OF THE VSCS

VSC	Rated power (MVA)	Initial power (MW)
1	100	35 (import from the dc grid)
2	100	50 (export from the dc grid)
3	80	28 (export from the dc grid)
4	80	44 (import from the dc grid)

TABLE VI
GENERATOR COST CURVES FOR IEEE-39 BUS SYSTEM

Area	Gen	Cost curve
1	G10	$0.004P_1^2 + 0.2P_1 + 13$
2	G1	$0.01P_3^2 + 0.8P_3 + 20$
	G2	$0.04P_4^2 + 0.6P_4 + 22$
3	G8	$0.02P_1^2 + 0.9P_1 + 25$
	G9	$0.04P_4^2 + 0.8P_4 + 30$

TABLE VII
ADAPTIVE AND CBA DROOP GAINS

VSC	Adaptive droop gain ($\alpha = 0.98$)	CBA droop gain ($\alpha = 0.8$)
1	6.41	1.03
2	8.31	2.76
3	5.78	5.03

2) Adaptive Droop Versus CBA Droop Scheme: In this section, the adaptive droop scheme [15] and the CBA scheme were compared. The adaptive droop coefficients to share the burden according to the available headroom can be calculated by $\mathbb{R}'_j = \mathbb{R}^0_j \times (\mathcal{R}_{base}/\mathcal{H}_j)^{\alpha}$. This ensures that converters which are already operating very close to the operational limit would not try to share the burden of a lost converter. However, it is anticipated that the cost factor is not considered in adaptive droop scheme in comparison with the proposed CBA scheme when the contingency occurs.

Authorized licensed use limited to: University of Arkansas. Downloaded on March 01,2022 at 20:42:25 UTC from IEEE Xplore. Restrictions apply.

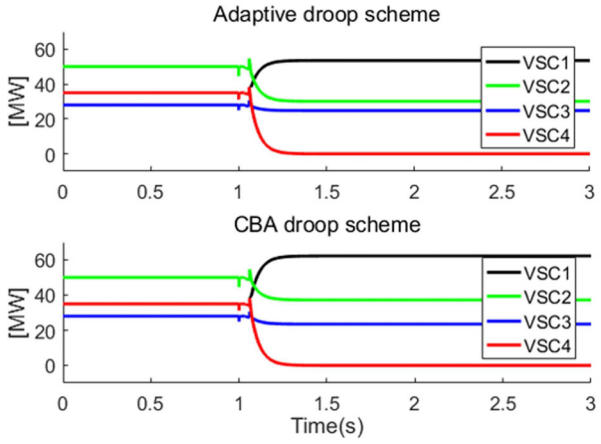

Fig. 12. Active power for the adaptive and CBA droop scheme following the outage of VSC4.

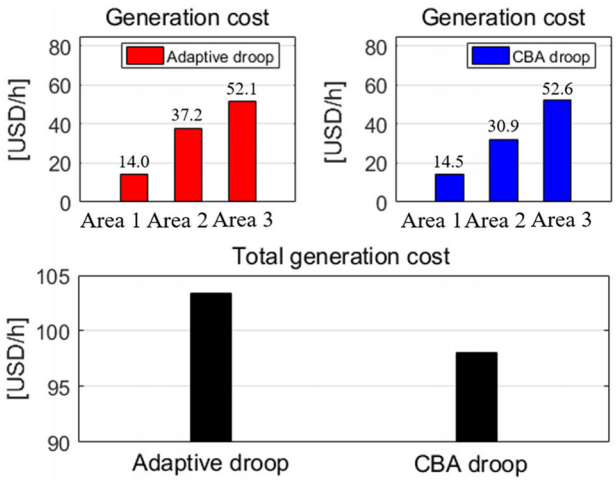

Fig. 13. Generation cost results.

Regarding the two kinds of droop control scheme, the initial droop gains are determined by $\mathbb{R}_1, \mathbb{R}_2, \mathbb{R}_3 = 3.5$ for converter performance, while considering the converter power ratings. Given that $P_l = 100$ MW, the λ_j^* is calculated as follows: $\lambda_1^* = 0.13$, $\lambda_2^* = 0.62$, $\lambda_3^* = 0.94$. Thus, the CBA droop coefficients $\mathbb{R}_1'$, $\mathbb{R}_2'$ and $\mathbb{R}_3'$ can be created by (26), as shown in Table VII. Considering the stable range of $\mathbb{R}_j'$, the user-defined positive constant α was set to 0.8. Accordingly, the CBA droop gains were updated to be $\mathbb{R}_1' = 1.03$ for VSC1, and $\mathbb{R}_2' = 2.76$ for VSC2, $\mathbb{R}_3' = 5.03$ for VSC3 in the economic dispatch cycle. Note that $\mathbb{R}_3'$ is calculated by $\mathcal{R}_{base} = 80$.

To validate the performance of the proposed droop scheme, the contingency time lines are as follows: 1) simulation start: 0 s, 2) apply 1-phase fault at bus 21: 1 s, 3) trip lines and VSC4 outage: 1.083 s, 4) simulation end: 3.0 s. And, the active power flow of VSC2 and 3 is indicated by positive values to enlarge the y-axis range.

Notable results of this scenario involved the active power from VSC1. In the CBA droop scheme, VSC1 which has a lower cost factor $\mathcal{F}_j$ value than VSC2 and 3 increases its power to the MTDC grids by a greater value, since the incremental cost in the power market of area 1 is low. In contrast, the adaptive droop gains are only determined by available headroom therefore a smaller amount of active power is injected into the MTDC grid than the CBA scheme. As shown by the black trace in Fig. 12, VSC1 increases its power to the MTDC grids from 35 MW to 61.2 MW in CBA droop scheme, while VSC1 increase its power from 35 MW to 53 MW in the adaptive droop scheme. However, total generation cost of area 1 between two control strategies is similar because of the relatively inexpensive generation cost in area 1.

Due to the similar converter headroom, the interval between adaptive droop gains is narrower than that in the CBA droop scheme, as shown in Table VII. On the other hand, the CBA droop gain $\mathbb{R}_1'$ is much smaller than $\mathbb{R}_3'$ because VSC1 has the smallest cost factor. Therefore, the CBA droop strategy can reduce the total incremental cost from 103.35 UDS/h to 98.09 USD/h, as shown by the black bars in Fig. 13. Assuming that there is no change in power balance and generation constraint for five hours, the CBA droop scheme can apparently reduce the total cost by approximately 26.28 USD more than the adaptive droop scheme. Therefore, the generation cost for the three ac systems can be reduced more than using the adaptive droop control strategy, and it should be noted that the post-contingency-steady-state operating point results are consistent with the analytical values.

In conclusion, the main differences between proposed and previous methods lie in whether a cost factor $\mathcal{F}_j$ value has been applied. If the areas have a high short-circuit ratio, while having a sufficient power reserve, the MTDC using the proposed CBA strategy has an appealing advantage of having the ability to operate economically by a simple formula. Notably, in practice, the droop gain range of the outer controller will be limited, and depending upon the connected ac grids or MTDC topology, the control variable α should be sufficiently chosen.

V. Conclusion

To date, there have been various studies examining autonomous power sharing in MTDC systems using adaptive droop control strategies instead of the fixed droop strategy. In this study, a CBA droop control scheme to reduce the total generation cost of the ac system is proposed. The advantage of this CBA droop control strategy is the fact that it considers the generator cost function of ac systems, while achieving robust control. The analytical derivation is established through transient simulations on an MTDC grid with four monopole VSCs, and the results for the rectifier outage under two different cost list scenarios are presented. The results present that the CBA droop achieved a greater reduction in active power generation costs compared to the fixed droop at post-contingency-steady-state operation points. The results indicate that the CBA droop scheme can be implemented effectively.

References

[1] J. Beerten and R. Belmans, "Modeling and control of multi-terminal VSC HVDC systems," *Energy Procedia*, vol. 24, pp. 123–130, 2012.
[2] L. Livermore, J. Liang, and J. Ekanayake, "MTDC VSC technology and its applications for wind power," in *Proc. 45th Int. Universities Power Eng. Conf. UPEC2010*, 2010, pp. 1–6: IEEE.

Authorized licensed use limited to: University of Arkansas. Downloaded on March 01,2022 at 20:42:25 UTC from IEEE Xplore. Restrictions apply.

[3] X. Chen *et al.*, "Integrating wind farm to the grid using hybrid multiterminal HVDC technology," *IEEE Trans. Ind. Appl.*, vol. 47, no. 2, pp. 965–972, 2011.
[4] N. R. Chaudhuri, R. Majumder, B. Chaudhuri, J. Pan, and R. Nuqui, "Modeling and stability analysis of MTDC grids for offshore wind farms: A case study on the North Sea benchmark system," in *Proc. IEEE Power Energy Soc. Gener. Meeting*, 2011, pp. 1–7.
[5] G. Bathurst and P. Bordignan, "Delivery of the Nan'ao multi-terminal VSC-HVDC system," in *Proc. 11th IET Int. Conf. AC DC Power Transmiss.*, 2015, pp. 1–6.
[6] C. Li, X. Hu, J. Guo, and J. Liang, "The DC grid reliability and cost evaluation with Zhoushan five-terminal HVDC case study," in *Proc. 50th Int. Universities Power Eng. Conf. (UPEC)*, 2015, pp. 1–6.
[7] X. Dianguo, L. Yuchao, and W. Jian, "Review on control strategies of multiterminal direct current transmission system," *Trans. China ElectroTech. Soc.*, vol. 30, no. 17, pp. 1–12, 2015.
[8] C. Dierckxsens, K. Srivastava, M. Reza, S. Cole, J. Beerten, and R. Belmans, "A distributed DC voltage control method for VSC MTDC systems," *Electric Power Syst. Res.*, vol. 82, no. 1, pp. 54–58, 2012.
[9] J. Beerten, D. Van Hertem, and R. Belmans, "VSC MTDC systems with a distributed DC voltage control-A power flow approach," in *Proc. IEEE Trondheim PowerTech*, 2011, pp. 1–6: IEEE.
[10] T. M. Haileselassie and K. Uhlen, "Impact of DC line voltage drops on power flow of MTDC using droop control," *IEEE Trans. Power Syst.*, vol. 27, no. 3, pp. 1441–1449, 2012.
[11] M. Hu, C. Fu, J. Wang, X. Li, and H. Liu, "Analysis on a parallel four-terminal HVDC transmission system based on real time digital simulation [J]," *Automat. Electric Power Syst.*, vol. 37, no. 5, pp. 87–92, 2013.
[12] C. Spallarossa, T. Green, C. Lin, and X. Wu, "A DC voltage control strategy for MMC MTDC grids incorporating multiple master stations," in *Proc. IEEE PES T&D Conf. Expo.*, 2014, pp. 1–5.
[13] T. Nakajima and S. Irokawa, "A control system for HVDC transmission by voltage sourced converters," in *Proc. IEEE Power Eng. Soc. Summer Meeting. Conf. (Cat. No. 99CH36364)*, 1999, vol. 2, pp. 1113–1119.
[14] A. S. Abdel-Khalik, A. M. Massoud, A. A. Elserougi, and S. Ahmed, "Optimum power transmission-based droop control design for multi-terminal HVDC of offshore wind farms," *IEEE Trans. Power Syst.*, vol. 28, no. 3, pp. 3401–3409, 2013.
[15] N. R. Chaudhuri and B. Chaudhuri, "Adaptive droop control for effective power sharing in multi-terminal DC (MTDC) grids," *IEEE Trans. Power Syst.*, vol. 28, no. 1, pp. 21–29, 2013.
[16] Z. P. Cheng, Y. F. Wang, Z. W. Li, and J. F. Gao, "DC voltage margin adaptive droop control strategy of VSC-MTDC systems," *J. Eng.*, 2018.
[17] J. Khazaei, Z. Miao, L. Piyasinghe, and L. Fan, "Minimizing DC system loss in multi-terminal HVDC systems through adaptive droop control," *Electric Power Syst. Res.*, vol. 126, pp. 78–86, 2015.
[18] W. Wang, Y. Li, Y. Cao, U. Häger, and C. Rehtanz, "Adaptive droop control of VSC-MTDC system for frequency support and power sharing," *IEEE Trans. Power Syst.*, vol. 33, no. 2, pp. 1264–1274, 2018.
[19] A. Yogarathinam and N. R. Chaudhuri, "Stability-constrained adaptive droop for power sharing in AC-MTDC grids," *IEEE Trans. Power Syst.*, vol. 34, no. 3, pp. 1955–1965, 2019.
[20] P. H. Divshali, S. H. Hosseinian, and M. Abedi, "A novel multi-stage fuel cost minimization in a VSC-based microgrid considering stability, frequency, and voltage constraints," *IEEE Trans. Power Syst.*, vol. 28, no. 2, pp. 931–939, 2012.
[21] E. Barklund, N. Pogaku, M. Prodanovic, C. Hernandez-Aramburo, and T. C. Green, "Energy management in autonomous microgrid using stability-constrained droop control of inverters," *IEEE Trans. Power Electron.*, vol. 23, no. 5, pp. 2346–2352, 2008.
[22] H. K. A. Alsiraji and E. F. El-Saadany, "Cooperative autonomous control for active power sharing in multi-terminal VSC-HVDC," *Int. J. Process Syst. Eng.*, vol. 2, no. 4, pp. 303–319, 2014.
[23] P. H. Divshali, A. Alimardani, S. H. Hosseinian, and M. Abedi, "Decentralized cooperative control strategy of microsources for stabilizing autonomous VSC-based microgrids," *IEEE Trans. Power Syst.*, vol. 27, no. 4, pp. 1949–1959, 2012.
[24] S. Cole, J. Beerten, and R. Belmans, "Generalized dynamic VSC MTDC model for power system stability studies," *IEEE Trans. Power Syst.*, vol. 25, no. 3, pp. 1655–1662, 2010.
[25] M. Cespedes and J. Sun, "Impedance modeling and analysis of grid-connected voltage-source converters," *IEEE Trans. Power Electron.*, vol. 29, no. 3, pp. 1254–1261, 2013.
[26] G. Binetti, A. Davoudi, F. L. Lewis, D. Naso, and B. Turchiano, "Distributed consensus-based economic dispatch with transmission losses," *IEEE Trans. Power Syst.*, vol. 29, no. 4, pp. 1711–1720, 2014.
[27] N. Rahbari-Asr, U. Ojha, Z. Zhang, and M.-Y. Chow, "Incremental welfare consensus algorithm for cooperative distributed generation/demand response in smart grid," *IEEE Trans. Smart Grid*, vol. 5, no. 6, pp. 2836–2845, 2014.
[28] F. Chen *et al.*, "Cost-based droop schemes for economic dispatch in islanded microgrids," *IEEE Trans. Smart Grid*, vol. 8, no. 1, pp. 63–74, 2017.
[29] Y. Huang, X. Yuan, J. Hu, and P. Zhou, "Modeling of VSC connected to weak grid for stability analysis of DC-link voltage control," *IEEE J. Emerg. Sel. Topics Power Electron.*, vol. 3, no. 4, pp. 1193–1204, 2015.
[30] H. Ding, S. Fan, J. Z. Zhou, Y. Zhang, and A. M. Gole, "Parametric analysis of the stability of VSC-HVDC converters," 2015.
[31] Y. Huang and D. Wang, "Effect of control-loops interactions on power stability limits of VSC integrated to AC system," *IEEE Trans. Power Del.*, vol. 33, no. 1, pp. 301–310, 2017.

Sungyoon Song (Student Member, IEEE) received the B.S degree in electrical engineering from Soongsil University. He received unified M.S. and Ph.D. degree in electrical engineering from Korea University, Seoul, Korea, in 2015, 2020. He has contributed to a wide variety of researches on the VSC-HVDC, FACTS system design and dynamic control. Also his research interests include probability power flow calculation using python script.

Roy A. McCann (Senior Member, IEEE) received the B.S. and M.S. degrees in electrical engineering from the University of Illinois at Urbana–Champaign, Champaign, IL, USA, in 1990 and 1991, respectively, and the Ph.D. degree in electrical engineering from the University of Dayton, Dayton, OH, USA, in 2001. From 1991 to 1994 he was a Design Engineer with General Motors. From 1994 to 1998, he was a Senior Project Engineer with ITT Automotive. From 1998 to 2003, he was with Delphi Automotive, Saginaw, MI, USA. He joined the Faculty of the University of Arkansas, Fayetteville, AR, USA, in 2003 and is currently a Professor with the Department of Electrical Engineering and Director of the Power Systems Control Laboratory. He is an Inventor on 20 U.S. patents and has published over 100 technical articles. His research is in the areas of modeling and control of large-scale renewable energy systems, power electronics, and electrical machinery.

Gilsoo Jang (Senior Member, IEEE) received the B.S. and M.S. degrees from Korea University, Republic of Korea. He received the Ph.D. degree from Iowa State University, U.S., in 1997. He worked in the Electrical and Computer Engineering Department at Iowa State University as a Visiting Scientist for one year, and as a Researcher at the Korea Electric Power Research Institute for two years. He is presently a Professor of the School of Electrical Engineering at Korea University. His research interests include power quality and power-system control.

Authorized licensed use limited to: University of Arkansas. Downloaded on March 01,2022 at 20:42:25 UTC from IEEE Xplore. Restrictions apply.